Nanoscale

Accepted Manuscript

Nanoscale

ARTICLE

Ligand effect on size, valence state and red/near infrared photoluminescence of bidentate thiol gold nanoclusters

Xavier Le Guevel[a*], Oya Tagit[b], Carlos E Rodríguez[c], Vanessa Trouillet[d], Manuel Pernia Leal[e], Niko Hildebrandt[b].

Synthesis and characterization of gold nanoclusters (Au NCs) stabilized by a zwitterion ligand (Zw) at different Au:Zw ratios is demonstrated. Au NCs exhibit photoluminescence (PL) emission, which is tunable from the near infrared (805 nm) to the red spectral window (640 nm) and strongly influenced by the ligand shell size. Optical and chemical investigations suggest the presence of gold polymeric species and large nanoclusters for a molar ratio of Au:Zw = 1:1. For 1:5 < Au:Zw < 1:1, Zw induces etching of the large clusters and the formation of a monolayer of the bidentate ligands on the Au NCs (clusters size ~ 7 to 10 kDa) accompanied by a red PL emission at λ = 710 nm. A second organic layer starts to form for larger Zw fractions (Au:Zw < 1:5) as a result of electrostatic and covalent interactions of the zwitterion leading to an enhancement and a blue-shift of the PL emission. Effect of temperature and pH on the optical properties of gold clusters is strongly dependent of the ligand shell and demonstrates the importance to define gold nanoclusters as supramolecular assemblies with a complex environment.

Introduction

Noble metal nanoclusters (NCs) with sizes approaching the Fermi wavelength of an electron (< 1nm) have gained much interest due to their various applications in catalysis[1] and optics[2], or in nanomedicine, where they have been used as biosensors[3-5] and bioimaging probes[6-9]. NCs differ from nanoparticles (NPs, diameter > 2 nm for gold) as they do not exhibit surface plasmon resonance but show discrete electronic states and molecular properties with an enhanced HOMO-LUMO gap[10-12]. This aspect leads to the emergence of new properties like magnetism[13], chilarity[14, 15] and photoluminescence (PL)[12]. During the last five years, many articles have reported the synthesis of fluorescent gold and silver NCs, emitting from the ultraviolet (UV) to the near infrared (NIR) wavelength range, by wet chemistry using thiol complexes[16-18], polymers[19-22] or biological scaffolds like DNA[23-25], peptides[7, 26, 27], enzymes[28] or proteins[29-33]. Great efforts have been made to understand the origin of the PL and to correlate it to the structure of those nanomolecules[11, 12, 30, 34]. Thiolate-Au NCs, also called gold thiolate-monolayer protected clusters (MPC), are among the best-characterized noble metal clusters, mainly due to improvements in their synthesis as

monodisperse single species[35-37]. Many studies have explored their structural, electronic and optical properties, also showing good correlations to time-dependent density functional theory (TDDFT) calculations[38, 39]. For instance, extensive investigations by mass spectrometry demonstrated the stability of specific sizes of Au NCs made by atomic packing in the gold core and stabilized by -S-Au-S- staples motifs: $Au_{25}(SR)_{18}$[16, 40, 41], $Au_{38}(SR)_{24}$[42-45], $Au_{67}(SR)_{35}$[46], $Au_{102}(SR)_{44}$[47], $Au_{144}(SR)_{60}$[18] with R= SCH_2CH_2Ph. Other studies investigated the influence of the ligand type on PL properties especially in the red-NIR wavelength region[17, 48, 49]. The extensive work on Au NCs using the ligand glutathione also demonstrated the role of valence state effects to the PL[50].

Among the thiol linker family, bidentate thiol molecules have been identified as interesting surface ligands due to their improved stability in biological media. For example, metal NPs and semiconductor quantum dots (QDs) have been used for bioimaging applications using such ligands[51-54]. Taking advantage of bidentate thiolate linkers, fluorescent gold and silver NCs synthesized with dihydrolipoic acid have revealed a relatively high and stable PL in the red region, which makes them very interesting candidates for biological investigations[6, 20, 55]. Recently, fluorescent gold and silver NCs

protected by other bidentate thiol ligands (zwitterion, modified-polyethyleneglycol) have shown remarkable optical properties with an intense PL (QY~14%) in a wide pH range[56-58].

In this work, we provide a detailed investigation of zwitterion-modified NCs with tunable PL emission wavelengths. By systematically varying the zwitterionic ligand content, we show their influence on growth, valence state and PL properties of the NCs (Scheme). Steady-state and time-resolved PL spectroscopy at different temperatures and pH revealed the contribution of energy transfer occurring in the core and on the surface of the NCs. These findings are highly important for a better understanding of the origin of the PL in the red and NIR wavelength region. Because multiple ligand layers seem to play a key role in NC properties, our results also provide useful information to hypothesize on a new model defining metal NCs as supramolecular assemblies.
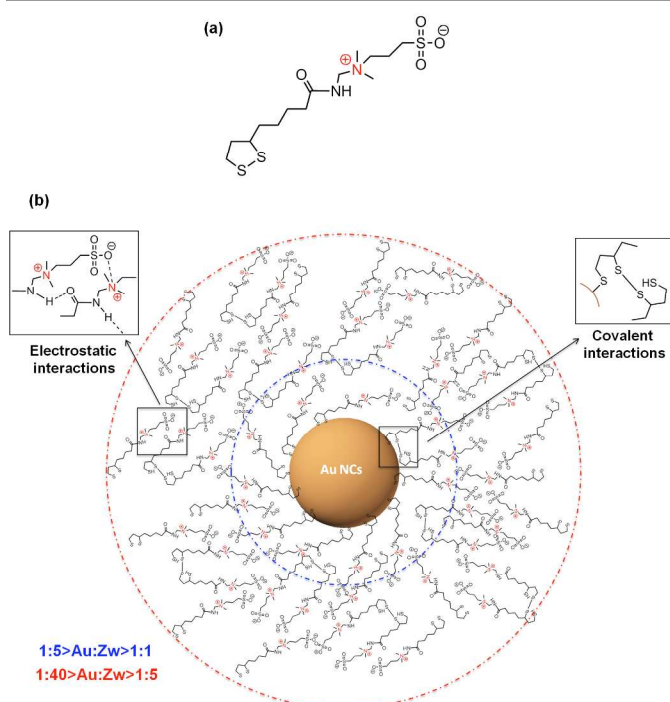
Scheme of (a) the zwitterion molecule (Zw) and (b) the gold nanoclusters protected by the ligand Zw.

Results

A Effect of the ligand on the size and the valence of Au NCs

The contribution of the organic part of AuZw on the size and valence of the NCs was determined by thermogravimetry for each Au:Zw ratio (from 1:1 to 1: 40) between 30°C and 850°C. Results (Table S1) indicate a linear increase of the ligand concentration from 53 wt% for Au:Zw 1:1 to 89.3 wt% for Au:Zw 1:40. The increase in the sulfur concentration with respect to gold as determined by elemental analysis and confirmed by XPS measurements demonstrates the high efficiency (low loss of ligand supplied during the synthesis) of ligand coating (Table 1).

Table 1. Determination of Au:S molar ratio in AuZw samples by XPS and by elemental analysis (ICP-OES).

	Au:S by XPS	Au:S by ICP
AuZw 1:1	1: 3.8	1: 2.9
AuZw 1:3	1: 6.0	1: 3.6
AuZw 1:5	1: 6.5	1: 5.2
AuZw 1:20	1: 20.7	1: 16.2
AuZw 1:40	1: 38.7	1: 42.7

Differential Thermal Gravimetry (DTG) analysis of the Zw ligand (Fig. 1 left) presents a band around 100°C associated to the loss of physisorbed water. The peaks observed at ca. 340°C and 540°C are both attributed to the decomposition of the organic compound. In the presence of gold, a peak located around 240°C is observed, which becomes more pronounced when the ligand content increases. This peak is usually attributed to the formation of self-assembled thiol monolayer clusters from the free thiol species[59, 60]. Interestingly, a new peak located at ca. 600°C appears for all AuZw samples. This band is shifted to lower temperatures for low Au:Zw ratios (Zw > 5). Because this peak is also associated to a sharp exothermic peak obtained with DSC measurements (Fig. 1 right), it can be attributed to the strong binding of Zw to the gold surface (delayed band of Zw at 540°C) or to the melting of Au NCs, which are known to be less stable than nanoparticles (size > 3 nm). In addition, it should be noted that only the sample AuZw 1:1 presents an additional band at 400°C. This behaviour might be caused by the formation of -Zw-Au-Zw-polymeric species at this molar ratio, instead of homogeneous NCs.

Although TEM measurements may lead to particle aggregation and are therefore not ideal for an exact NC size determination, the AuZw NCs showed relatively monodisperse species with sizes below 2 nm and the absence of large (> 3 nm) nanoparticles (Fig. S4).

MALDI-TOF experiments were performed to investigate the effect of the ligand on the size of the Au NCs. Linear positive mode at high-energy measurements obtained for AuZw are depicted in Fig. 2. The continuous band centered at ~14.5 kDa m/z for AuZw 1:1 corresponds to the contribution of the ligand Zw associated to the Au NCs. When the amount of ligand increases, there is a shift to higher mass (~19 kDa for AuZw 1:3). Further decrease of the Au:Zw ratio (1:20 and 1:40) leads to significant broadening of the band due to the contribution of the organic moiety (Fig. S5).

Fragmented Au NCs were detected at lower mass and the signal is transformed from a continuous band to discrete characteristic peaks showing Gaussian forms and equal spacing. The m/z = 197 and m/z= 32 peaks correspond to the loss of one gold atom and one sulfur, respectively (Fig. S6). It should be mentioned that numerous attempts to obtain non-fragmented Au NCs species without the loss of ligands by using graphene as co-matrix[61] with CHCA or with the matrix trans-2-[3-(4-tert-

butylphenyl)-2-methyl-2-propenylidene]malononitrile (DCTB)[16, 62, 63] were revealed to be unfortunately unsuccessful.
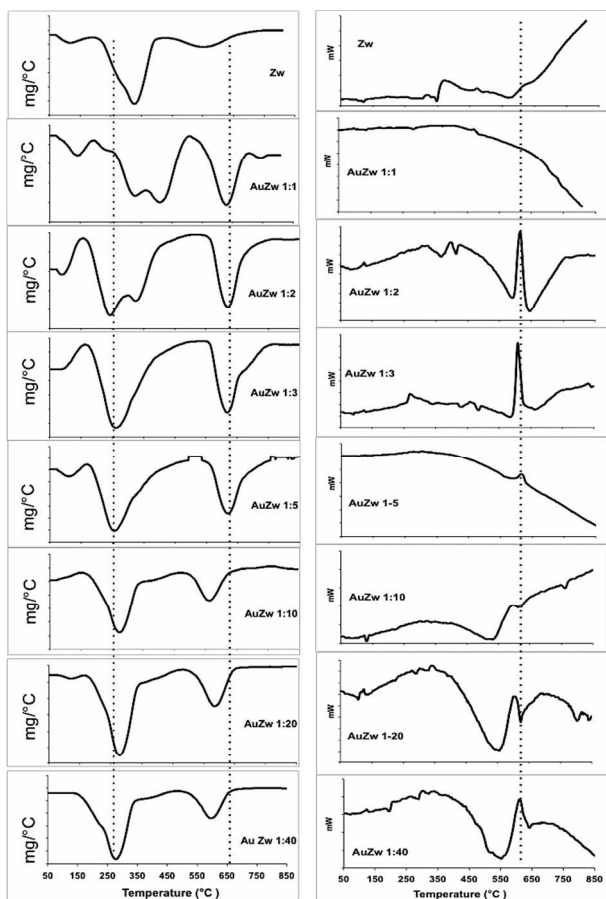

Fig. 1. Differential thermogravimetry (on the left) and differential scanning calorimetry (on the right) of AuZw samples at different Au:Zw ratios.

However, the experiments performed under equal conditions for all samples suggest a clear modification of the distribution of the fragmented Au NCs when the Au:Zw ratio decreases from 1:1 to 1:3. As shown in Fig. 2, peaks beyond ca. 7 kDa significantly decrease and disappear in the background signal for masses between ~13 to 17 kDa when changing from 1:1 to 1:3. No difference of the peaks related to Au NCs was identified for lower Au:Zw ratios with a maximum of species centered around 7 kDa and at lower proportion around 9 kDa. These measurements suggest an etching process when the Au:Zw ratio decreases from 1:1 to 1:3. At lower ratios of Au:Zw, no significant impact of the ligand content on the clusters size is observed.

The fluorescent bands obtained with AuZw on the separation gel by PAGE (Fig. S7) show a distribution of PL between 10 kDa and 20 kDa with the highest intensity at ~10 kDa, which is an agreement with the NCs size determined by mass spectrometry.
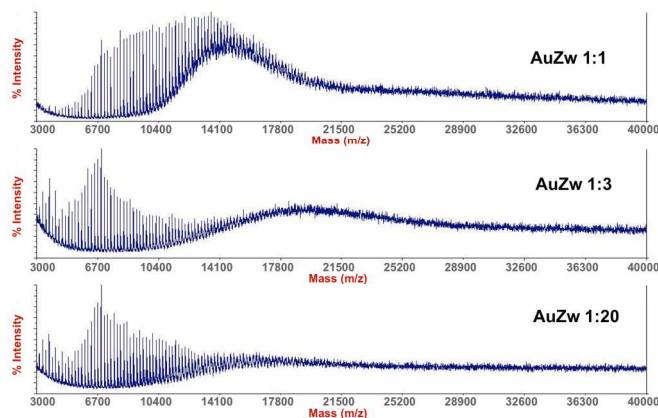

Fig. 2. MALDI-TOF patterns of AuZw samples at different Au:Zw ratios in linear positive mode at high energy using CHCA as matrix. The broad band corresponding to the complete Au NCs assembly- associated to the ligand by covalent and no covalent bonds- shifts to a higher molecular weight for high ligand content. Discrete peaks attributed to the fragmented Au NCs core- without the outer shell of non-covalent bond molecules- shift to a lower molecular weight by decreasing the ratio Au:Zw from 1:1 to 1:3.

The oxidation state of gold and of the sulfur groups were analyzed by XPS measurements (Fig. S8). The binding energy of $Au4f_{7/2}$ for AuZw can be deconvoluted in two distinct bands: one located at 84.0 eV corresponding to Au(0) and the second one at 84.7 eV, which can be attributed to partially-oxidized gold atoms[26, 64, 65]. The ratio Au(84.7 eV)/Au(84.0 eV) is almost constant for AuZw 1:1; 1:3 and 1:5 (see Table 2) and increases for AuZw 1:20 suggesting that the thiol groups of Zw are still reacting with the Au NCs between 1:5 and 1:20. The XPS data of sulfur provides information on the binding of the thiol ligand Zw to the Au NCs, the presence of free thiol and the concentration of the ligand with respect to Au concentration. The ratio of S bound to hydrogen/carbon (i.e free thiols) at 163.5 eV to S bound to metal at 162.0 eV reported in Table 2 increases with the number of Zw per gold atoms. In the sample AuZw 1:1, no doublet at 163.5 eV is observed indicating a complete reaction between the ligand to the gold. Then, the intensity of this peak increases showing the presence of free thiol surrounding the Au NCs. The reduced increase of free thiol and the increase of the ratio Au(84.7 eV)/Au(84.0 eV) between the samples AuZw 1:5 and AuZw 1:20 might confirm the saturation of thiol binding to the surface of Au NCs. The saturation of the ratio Au(84.7 eV)/Au(84.0 eV) and the continuous increase of the sulfur group for AuZw 1:40 can be associated to the additional crosslinking of the ligand to the Zw monolayer stabilizing the Au NCs.

Table 2. Data extracted from XPS Au 4f and S 2p spectra of AuZw samples prepared at different Au:Zw ratio.* values $\in$[1.5-3.2]

	Au(84.7 eV)/Au(84.0 eV)	$S_{bound\ to\ C/H}$ (163.5 eV)/$S_{bond\ to\ Au}$ (162.0 eV)
AuZw 1:1	1.9±0.1	0
AuZw 1:3	1.8±0.1	4.6±0.1
AuZw 1:5	1.9±0.1	4.7±0.1
AuZw 1:20	3.3±0.1	6.5±0.1
AuZw 1:40	-*	13.5±0.1

B Effect of the ligand on the photophysical properties of Au NCs

Optical absorption spectra of AuZw at different Au:Zw molar ratios (Fig. S9) show a continuous decrease of absorbance with increasing ligand concentration resulting in a color change from a dark brown for Au:Zw with Zw < 10 to pale yellow for Zw ≥ 10. We did not observe any plasmon bands at 520 nm (characteristic for gold NPs) but broad absorption bands around 510 nm (2.43 eV), 590 nm (2.10 eV), 700 nm (1.77 eV) and 820 nm (1.51 eV), which are commonly related to the intra and inter-band energy transitions of Au NCs[34]. Reduced absorption of the bands at 700 nm and 800 nm was observed when the Au:Zw ratio decreased from 1:1 to 1:3 and these bands completely disappear for higher ligand concentrations. The band at 590 nm decreases as the Au:Zw ratio decreases from 1:1 to 1:5 and is completely absent for 1:10 to 1:40 samples, most probably due to the oxidation of the clusters[66].

PL emission spectra of highly diluted AuZw NCs (O.D. < 0.15 at λ = 450 nm) at the same gold concentration were measured at pH 7 and 20°C (Fig. 3a and b). It should be mentioned that the ligand Zw does not emit in the red-NIR region. UV excitation was not used in order to prevent energy transfer between the Zw ligand and the Au NCs. The fluorescence spectra show a peak centered around 805 nm (*band I*). The intensity of *band I* increases with increasing ligand concentration until a saturation is reached for Au:Zw = 1:5 (see Fig. 3a, b and d). A second maximum, whose intensity also increases from Au:Zw 1:1 to 1:5, appears at ca. 710 nm (*band II*). The intensity of *band II* increases significantly stronger compared to *band I*. In contrast to previous PL studies on AuZw[56], we clearly observed (in many repeated experiments) an intensity enhancement and significant blue-shift (more than 50 nm) of the PL emission *band II* for high ligand contents (ratio Au:Zw with Zw > 5), which was independent of the excitation wavelengths (680 nm for AuZw 1:10, 670 nm for AuZw 1:20, and 660 nm for AuZw 1:40). Even higher ligand concentrations during synthesis (not shown) leads to a further blue-shift and a broadening of the emission wavelength at 640 nm and an intensity decrease, most probably due to aggregation of the ligand at such high concentration in solution.

In agreement with the absorption spectra, the PL excitation spectra of AuZw exhibit multiple discrete bands at: 370 nm (3.35 eV), 405 nm (3.06 eV), 445 nm (2.79 eV), 470 nm (2.64 eV), 495 nm (2.50 eV), 515 nm (2.41 eV) (Fig. 3c). Although these multiple bands are also superposed to a continuously decreasing spectrum from the UV to the NIR, the maxima are better visible compared to the absorption spectra. In contrast to

the absorption spectra, the intensity of the PL emission and excitation spectra increase with increasing ligand concentration. The strong absorption of AuZw with lower organic content (Fig. S9) must be caused by non-emitting species and might be partially attributed to the presence of the polymeric species – Zw-Au-Zw and aggregation of large clusters. Increasing the Zw ligand concentration has therefore two advantages for PL measurements: it decreases the absorption of non-emitting species (and therefore the reabsorption of the PL emission) and increases the PL intensities. Higher ligand concentrations for the samples with Au:Zw ratio 1:5 to 1:40 result in a pronounced enhancement of the excitation peaks at 470 nm and 495 nm when measuring an emission wavelength in the red range (640 nm and 700 nm). This indicates the presence of a strong coupling of the emitters at $\lambda_{exc.}$= 495nm / $\lambda_{em.}$ $\in$ [640-700nm]. PL quantum yields of AuZw at different ratios were calculated by comparison to Rhodamine 6G and show an increase with the amount of organic content from 0.8% for AuZw 1:1 to 15% for AuZw 1:40 (Table S2).
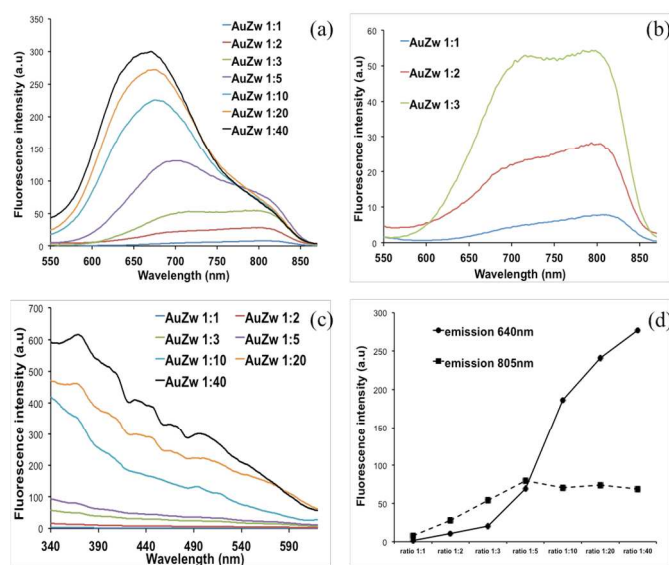

Fig. 3. Photoluminescence (PL) emission* (a, b) and excitation** (c) spectra of AuZw at different Au:Zw ratios. (d) Evolution of the PL intensity at $\lambda_{em.}$= 640 nm and 805 nm as a function of Au:Zw ratio. *$\lambda_{exc.}$= 450 nm. **$\lambda_{em.}$= 640 nm.

In order to understand the contribution of the ligand content to the modification of the PL properties, we measured the PL emission at varying pH, temperature, and reduce conditions. PL spectra of AuZw NCs were measured for a wide range of pH (pH 3 to 11, cf. Fig. 4a and Fig. S10). For all samples the highest PL intensity is observed at basic pH, decreasing toward acidic conditions. *Band II* (lower wavelength band) is more sensitive to pH than *band I*, a trend that is most clearly observed for Au:Zw with Zw< 5. Compared to the high ligand concentrations (1:20 and 1:40), AuZw samples with lower Zw content (Au:Zw 1:2, 1:3, and 1:5) are much less prone to pH changes from pH 4 to 11 and only show a strongly decreased

intensity for pH 3. PL spectra were also recorded for different temperatures: 5, 10, 20, 37 and 50°C. Both *band I* and *band II* decrease with increasing temperature and *band I* is slightly less affected than *band II* (Fig. 4b and Fig. S11). High ligand concentrations in solution might lead to strong electrostatic and covalent interactions between the ligands. In order to evaluate the effect of ligand interaction on the photophysical properties of Au NCs, a concentrated solution of reducing agent was added to AuZw with high ligand content (AuZw 1:40 and AuZw 1:60) to break the disulfide bonds between cross-linked zwitterions. Free ligands were then removed by filtration. This procedure can be viewed as a "peeling process" to remove the ligand not directly bond to the metal core. Fig. 4c and Fig. S12 show a significant decrease of PL intensity mainly in the 600 to 650 nm wavelength range leading to a PL emission spectrum similar to AuZw 1:10. The control experiment with AuZw 1:3 sample (Fig. 4d) only led to significant PL intensity changes at very high contents of reducing agent. These "inverse" ligand-detachment experiments demonstrate the impact of the removal of ligands from AuZw on the Au NC PL properties.

shorter one with $\tau_2 \sim$ 0.1-0.3 µs, which both do not significantly change with varying excitation/emission wavelengths. However, their amplitude fractions are dependent on the emission wavelength (Fig. 5c). For the three selected excitation wavelengths the amplitude fractions a_1 of the longer components increase with increasing emission wavelength (and the amplitude fractions a_2 of the shorter components decrease). Moreover, the average PL decaytime $<\tau>_i = (a_1\tau_1^2 + a_2\tau_2^2) / (a_1\tau_1 + a_2\tau_2)$ decreases with increasing sample temperature (Fig. 5d).
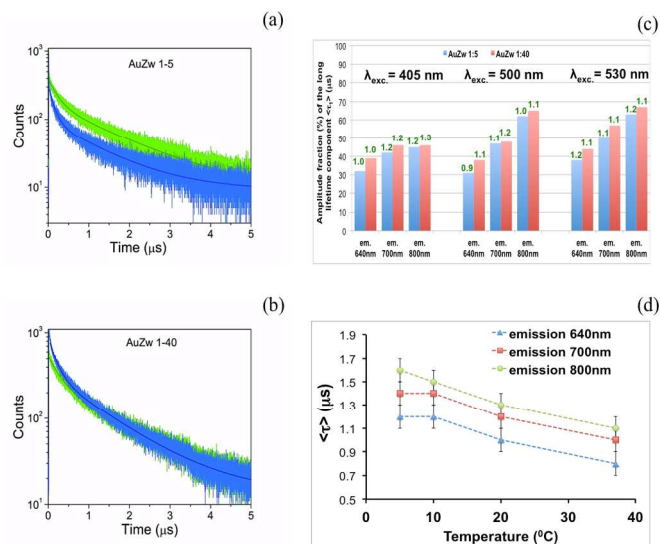
Figure 5. PL decay curves and corresponding fits (black lines) for AuZw 1:5 (a) and AuZw 1:40 (b) obtained at 640 nm (blue) and 800 nm (green) emission wavelengths using an excitation wavelength of λ_{exc} = 405 nm. (c) Amplitude fractions of the longer PL decay component (τ_1) of AuZw 1:5 and AuZw 1:40 at varying excitation and emission wavelengths. Average PL decaytimes are given on top of the bars. Sample temperatures for graphs a to c were 20° C. (d) Average PL decaytimes as a function of sample temperature for AuZw 1:40 using an excitation wavelength of λ_{exc} = 405 nm. More detailed decaytime data can be found in Figures S13/14 and Table S3.
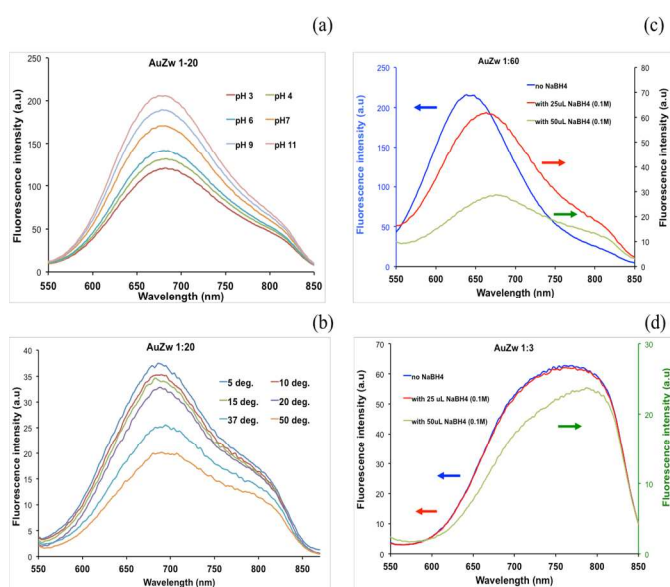

Fig. 4. Photoluminescence (PL) emission spectra* of AuZw 1:20 at different temperature (a) and pH (b). Evolution of the PL intensity* of AuZw 1:60 (c) and AuZw 1:3 (d) after two reducing cycles using NaBH₄ (0.1M). *λ_{exc} = 450 nm.

PL decaytime measurements were performed with Au:Zw 1:5 and Au:Zw 1:40 samples for different excitation/emission wavelengths and at different temperatures from 4°C to 37°C. In order to investigate the red and NIR PL decays, 640 nm, 700 nm and 800 nm were selected as PL emission wavelengths and the NCs were excited at λ= 405 nm, 500 nm and 530 nm. Representative decay curves collected at 640 nm and 800 nm are shown in Figures 4a and 4b for Au:Zw 1:5 and 1:40, respectively. The red/NIR PL decays of AuZw NCs (Fig. 5 and Table S3) are significantly longer compared to the visible (450 nm) decays (Figure S13). Their decay curves show two components, a longer one with $\tau_1 \sim$ 1-2 µs and a

Discussion

A Growth and ligand protection of Au NCs

Gold (I) is known to easily form complexes with thiol groups and it can lead to the formation of dimers, oligomers and nanoparticles in the presence of reducing agents. In the case of the compound AuZw 1:1, our results suggest the presence of multiple species in solution: i) polydisperse Au NCs (from 7 kDa to 17 kDa) detected by mass spectrometry (and even NPs as observed by TEM), and ii) polymeric species Zw-Au-Zw confirmed by XPS and thermal analysis. Increasing ligand contents (Au:Zw from 1:1 to 1:3) leads to an etching process of the big Au NCs species (with sizes around 13-17 kDa), which disappear from the mass spectra. The formation of Au NCs stabilized by a monolayer of the thiol bidentate ligand Zw was followed by the rise of metal-thiol binding and the evolution of

free thiol groups by different techniques (elemental analysis, thermogravimetry, mass spectrometry). The size distribution of Au NCs in the 7 kDa to 9 kDa range measured by mass spectrometry and electrophoresis does not seem to be affected by the increase of the ligand content suggesting a stability of the Au NCs core for Au:Zw = 1:3 and higher ligand contents. To confirm the total etching process, no NPs were identified by TEM but NCs with sizes of ~1 nm (< 100 atoms for gold). As already mentioned in the results section, the mass spectrometry peaks are associated to fragmented-charged Au NCs species and the determination of single stable Au NCs (in our case the ionic ligand Zw) was not successful. However, considering the extensive work on the structure and the optical properties of Au NCs stabilized by thiol molecules and the gel electrophoresis data, it is reasonable to associate the species at 7 kDa to 9 kDa, which exhibit red-NIR fluorescence emission, to NCs with a number of gold atoms below 100 and more likely with the presence of Au_{25}[15, 18, 26, 34, 37, 49].

XPS is a useful tool to determine the formation of monolayer protected metal nanoclusters. Tanaka et al. described how Au4f patterns can be deconvoluted in two bands at 84.0 eV corresponding to Au(0) probably located in the core of the NCs, and at an intermediary binding energy between Au(0) and Au(I) at 84.7 eV, which was reported as being associated to the gold in the outer part of the clusters stabilized by -R-Au-R- staples (R= ligand)[26]. Therefore, combining measurements of the free thiol concentration with respect to gold concentration by XPS and thermal analysis to the proportion of gold partially oxidized by XPS enabled us to follow the continuous process of ligand saturation around the Au NCs, which occurs at ratios of 1:10 < Au:Zw < 1:5. Additional Zw interactions with the saturated thiolate Au NCs via electrostatic (ammonium-sulfate) or covalent interactions (disulfide bonds) are expected to start already at ratios between 1:5 and 1:20, when the maximum ligand coverage on NCs (containing less than 100 atoms) is considered.

B Origin of PL in the red and NIR

PL emission of Au NCs in the red and NIR region has been reported in numerous papers and is commonly associated with metal-ligand and metal-metal charge transfer, which are related to interband (sp←d) and intraband (sp←sp) transitions[12]. No characteristic plasmon bands of gold NPs (at 520 nm) were detected for AuZw with a ratio of Au:Zw = 1:1, but the absorption spectrum shows the presence of absorption bands centered around 670 nm and 800 nm. Such optical characteristics were observed in different examples of Au NCs prepared in the presence of thiol ligands such as glutathione[26, 50, 67], mercaptosuccinic acid[68] or others thiol hydrophobic molecules[69] and are usually attributed to LUMO←HOMO and spin-forbidden transition, respectively[66]. The sample AuZw 1:1 exhibits a weak fluorescence at 805 nm (1.54eV, *band I*), which has been attributed in some cases to the energy transfer occurring in the Au NC core[13] or to metal-thiol polymeric complexes[50, 70]. When the amount of ligand increases, the *band I* intensity reaches a maximum for Au:Zw = 1:5 without any shift of the emission wavelength. *Band I* appears to be less sensitive than the red emission at 710 nm (*band II*) to temperature and pH. This observation seems to validate the hypothesis of a NIR emission originating from the core of the NCs and rather independent of external effects[44, 71, 72]. The etching of big clusters to small clusters inducing a quantum confinement with PL emission for this range of clusters size also supports this statement[12]. For example, Wen et al. demonstrated the contribution of the red emission and the NIR emission from the [− S− Au(I)− S− Au(I)− S−] staples and the Au_{13} core respectively by temperature-dependent PL for Au NCs stabilized by the protein BSA[72]. However, we cannot ignore the fact that polymeric species Zw-Au-Zw are formed for the ratio Au:Zw = 1:1, which could also be partially responsible for the NIR emission. Furthermore, the average PL decaytimes measured in this study are slightly increasing with increasing emission wavelengths, which is a typical signature of gold complexes without the contribution of any NCs or NPs.

When the ratio Au:Zw decreases from 1:1 to 1:5, there is a constant increase of PL intensity from *band II* indicating the formation Au NCs with the thiol monolayer of the ligand. This PL has been known to be associated to the metal-ligand transfer from the staple -R-Au-R-surrounding the core of the Au NCs[10, 13, 26, 73]. This layer enables a strong protection from the environment with almost no modification of the PL intensity in a wide range of pH. These PL properties are in agreement with previously described Au NCs stabilized by thiol bidentate linkers[55, 56, 58]. Interestingly, the contribution of the PL from *band II* differs at high ligand content. For the Au NCs with larger ligand shells (Au:Zw 1:20 and Au:Zw 1:40), a blue shift of the PL emission maximum band and a higher sensitivity to the pH is observed. In fact, it appears unlikely for Au:Zw 1:10, 1:20 and 1:40 that the intense red emission is only originating from the ligand bond to the Au NCs due to the full coverage of ligands on Au NCs surface[47]. Therefore, the PL enhancement and the blue-shift may rather be attributed to the formation of a second ligand layer, creating a protective dielectric shell around a densely packed thiolate-Au NCs species via electrostatic (ammonium-sulfate) and covalent (disulfide interaction) bonding (cf. Scheme). This hypothesis was confirmed by the "peeling experiment" aiming to break cross-linked zwitterions. Removing ligands from the outer layer led to a red-shifted PL emission with a slightly narrower bandwidth. Because the change of pH, temperature, or dilution does not alter the PL maximum in the red wavelength region we conclude that the organic layer, which protects the metal core, is relatively stable. Similar effects of the ligand shell on the optical properties of metallic nanoparticles and quantum dots have been reported[74-76]. Another study also showed PL enhancement of Ag clusters in a saturated solution of poly(ethyleneglycol) groups, demonstrating the linear increase of the PL intensity of Ag NCs with increasing amounts of polyethylene groups protecting the clusters from the environment[77]. Taking into account different reports demonstrating the solvathochromic properties of gold and silver NCs and their numerous applications for

sensing[12, 19, 78], the strong sensitivity of metal NCs to the environment was somewhat expected.

Several studies of Au NCs stabilized by bovine serum albumin (BSA) have provided crucial information about environmental effects on structure and optical properties of those NCs[30, 72, 73, 79]. Such clusters are mainly consisting of 25 atoms (icosahedral 13 Au(0) core stabilized by [−S−Au(I)−S−Au(I)−S−] staples) and are polarized in the structure of the biological template. They exhibit red PL emission with long decaytimes, strongly influenced by the electrostatic and covalent interactions with specific amino acids. AuBSA is a complex system, which makes it hard to fully understand the multiple mechanisms of charge transfer between the metal clusters and the template due to the large size (66.3 kDa) and the structure of BSA, and the localization of the Au NCs inside the protein. In contrast to AuBSA, AuZw is a simple model, in which controlled addition of a small ligand (412 Da) and a nearly unchanged NCs size (confirmed by mass spectrometry) allows the determination of the ligand-related contributions to PL emission. In the case of AuZw, the ligand content does not affect the lifetime properties indicating a relatively weak impact of the ligand shell to the nature of the energy transfer. These results support the idea of a second ligand shell acting as diffusion layer but not inducing a direct charge transfer to the core of the stabilized NCs.

Despite the good evidence for a correlation between the enhancement of the red PL and the growth of a second-or "larger"- ligand shell on the Au NCs, it remains challenging to study the origin of the PL from the core, the ligand-to-metal and the diffusion through the second ligand layer separately due to not only the multiple transfers occurring from the UV to the NIR window[40, 80], but also due to the process of NC formation in solution. Therefore, more investigations are required to determine precisely the growth steps of NCs in solutions and the nature of the second ligand shell to fully understand its role on the photophysical properties of this new class of PL emitters.

Materials and methods

Synthetic procedure

All products were purchased from Sigma Aldrich and MilliQ (Millipore, SPAIN) water was used for all experiments.

Lipoic acid-zwitterionic ligand (Zw) was synthesized following the procedure described elsewhere [81]. Infrared spectroscopy, NMR ^{1}H and mass spectrometry in reflective mode confirmed the purity of the compound (see ESI: Fig. S1-3). Au NCs were prepared with different molar ratios of Au per Zw (Au:Zw) from 1:1 to 1:60 in basic conditions in the presence of sodium borohydride as reducing agent. Briefly, in a standard experiment for the molar ratio **Au:Zw = 1:5**, 12.5 µmol (5.15 mg) of Zw was added to the basic mixture of 50 µL of HAuCl$_4$.3H$_2$O (50 mM) in 5 mL of deionized water and 10 µL of NaOH (2M) under stirring for 5 min. Then, 100 µL of

freshly prepared NaBH$_4$ (50 mM) was added to the solution and stirred for 15 hours. The solution changed quickly from colorless to brownish indicating the growth of Au NCs. Afterwards, solution containing AuZw NCs was purified twice using filters with 3kDa molecular weight cut-off (Amicon ultra, Millipore) to remove the excess of free ligands. The pH was adjusted to 7 and AuZw NC solution was kept refrigerated until use.

Regarding the "ligand peeling experiment", AuZw samples with low (AuZw 1:3) and high organic content (AuZw 1:40 and AuZw 1:60) were mixed with freshly prepared NaBH$_4$ (0.1M), vortexed and centrifuged at 13,000 rpm with a 3 kDa filter for 15min. Fluorescent measurements were then performed repeatedly after each reducing cycle.

Instrumentations

Chemical measurements. The freeze-dried samples were characterized by Infrared spectroscopy on a FTIR-4100 Jasco from 600 cm^{-1} to 4000 cm^{-1}. NMR measurement of the zwitterionic ligand (Zw) was performed on a NMR Bruker Ascend™ 400MHz. Concentration of gold and sulfur for each sample was estimated by inductively coupled plasma optical emission spectrometry (ICP-OES) on an OPTIMA 7300DV (Perkin Elmer) with detectors in the wavelength range between 163 nm and 782 nm. Concentrations were determined with the software WinLab32 (Perkin Elmer). Transmission electron microscopy (TEM) images of the NCs were measured on a FEI Tecnai G2 Twin TEM.

XPS investigation was performed in a K-Alpha spectrometer (ThermoFisher Scientific) using a microfocused, monochromated Al Kα X-ray source (200 µm spot size). The K-Alpha charge compensation system was employed during analysis, using electrons of 8 eV, and low-energy argon ions to prevent any localized charge build-up. The kinetic energy of the electrons was measured by a 180° hemispherical energy analyzer operated in constant analyzer energy mode (CAE) at 50 eV pass energy for elemental spectra. Data acquisition and processing using the Thermo Avantage software is described elsewhere[65]. The spectra were fitted with one or more Voigt profiles (BE uncertainty: ±0.2eV) and Scofield sensitivity factors were applied for quantification[82]. All spectra were referenced to the C1s peak at 285.0 eV binding energy (C-C, C-H) and controlled by means of the well-known photoelectron peaks of Cu, Ag, and Au, respectively. Measurements were performed on different locations of the solid and with different series of samples.

Evolution of the gold NCs size as a function of the ratio metal/ligand was determined by Matrix-assisted laser desorption/ionization (MALDI) on a 4700 Proteomics Analyzer Mass Spectrometer (ABSCIEX. Framingham, MA. USA). Samples were prepared with the matrix α-Cyano-4-hydroxycinnamic acid (CHCA), 5 mg/mL in 50% acetonitrile, 0,1% trifluoroacetic acid (TFA) with volume ratio 1:1. CHCA, acetonitrile and TFA were purchased from Sigma-Aldrich (St. Louis, Mo., USA). The samples were analyzed in *Linear middle mass positive ion mode:* 20 kV source 1 acceleration voltage. The Grid 1 voltage was set to 92.5% of the source 1

acceleration voltage. Delay time DE1 was 850 ns, and the low mass gate was enabled with an offset of 0.0. Each data point was the summation of 20 spectra, acquired with 50 laser shots each. External calibration was carried out with a set of synthetic peptides (Sequazyme Peptide Mass Standards Kit, Calibration Mixture 3, ABSCIEX).

Thermal analysis of the samples AuZw were performed by Thermogravimetry (TG), and differential scanning calorimetry (DSC) using a METTLER TOLEDO model TGA/DSC 1 between 30 and 850°C at 10°C/min with an air flux at 50 mL/min.

PAGE electrophoresis of the samples were measured using a 15% polyacrylamide gel with a Bio-Rad (Hercules, CA, USA) equipment at 100V for 90 min. 10 μL of glycerol was added to 20 μL of each concentrated samples in each well. Molecular weight was determined with a Precision Plus Protein Dual Xtra standard indicator™ (250 kDa-2 kDa).

Optical measurements. Absorption spectra were collected on a UV-visible spectrophotometer Cary 100Bio (Varian) in 190 nm - 900 nm range. Steady-state fluorescence measurements were obtained with diluted samples on a Perkin Elmer LS45 Fluorescence Spectrometer. PL decaytime measurements were performed at four different emission wavelengths (445 nm, 640 nm, 700 nm and 800 nm) using three different excitation wavelengths (405 nm, 500 nm and 530 nm) on a FluoTime 300 time-resolved fluorescence spectrometer (PicoQuant) equipped with a peltier temperature controller TC125 (Quantum Northwest). Sample temperatures were equilibrated for at least 30 minutes before the measurements. A picosecond pulsed diode laser EPL-405 (Edinburgh Instruments) (center wavelength 405±7 nm) operating at 0.2 MHz was used for the excitation of samples at 405 nm. Excitation of samples at 500 nm and 530 nm was achieved using a wavelength-tunable supercontinuum source SuperChrome (Fianium) operated at 0.2 MHz. Excitation power of the SuperChrome output beam was adjusted such that the count rates were equal to 405 nm excitation. Decay curves were fitted using FluoFit Pro version 4.4.1.0. (PicoQuant).

Conclusions

In this study, we investigated the bidentate thiol ligand-enabled formation of a mixture of species (polymeric gold complexes, NPs and NCs) exhibiting weak PL in the NIR region (λ = 805 nm). An increase of the ligand content leads to a rapid etching process of the big clusters followed by the formation of a first shell of thiol linkers bound to the gold NCs. This process is accompanied by the increase of red PL intensity at λ = 710 nm without affecting the core size ($\sim$ 7-10 kDa). A second ligand shell on the thiol-Au NCs induces a strong modification of the optical properties including PL enhancement and a blue-shift (> 50nm) of the PL emission. Our detailed investigation using chemical and photophysical characterization stresses the importance to carefully consider the macromolecular and complex environment-dependent

character of fluorescent metal NCs in order to fully understand and appreciate the photophysics and photochemistry of these novel nanoscale fluorophores.

Acknowledgements

Notes and references

[a] Therapeutic Nanosystem, Andalusian Centre for Nanomedicine and Biotechnology, BIONAND, Parque Tecnológico de Andalucía, Málaga, Spain.

[b] NanoBioPhotonics, Institut d'Electronique Fondamentale, Université Paris-Sud- 91405 Orsay Cedex, France.

[c] Molecular Basis of Cell Proliferation BIO267. Proteomics Unit of the SCBI, University of Málaga. Parque Tecnológico de Andalucía, Málaga, Spain.

[d] Institute for Applied Materials (IAM) and Karlsruhe Nano Micro Facility (KNMF), Karlsruhe Institute of Technology (KIT), Eggenstein-Leopoldshafen, Germany.

[e] Diagnostic Area, Andalusian Centre for Nanomedicine and Biotechnology, BIONAND (Junta de Andalucía-Universidad de Málaga), Parque Tecnológico de Andalucía, Málaga, Spain.

Electronic Supplementary Information (ESI) available: [spectroscopic characterization of the organic ligand and, microscopy, chemical and optical properties of the gold nanoclusters stabilized by the bidentate thiol ligand]. See DOI: 10.1039/b000000x/

1. Y. Zhu, H. Qian and R. Jin, *Journal of Materials Chemistry*, 2011, 21, 6793-6799.
2. A. S. Kuznetsov, V. K. Tikhomirov and V. V. Moshchalkov, *Optics Express*, 2012, 20, 21576-21582.
3. L. Shang and S. Dong, *Biosensors and Bioelectronics*, 2009, 24, 1569-1573.
4. H. C. Yeh, J. Sharma, J. J. Han, J. S. Martinez and J. H. Werner, *Nano Letters*, 2010, 10, 3106-3110.
5. Z. Yuan, M. Peng, Y. He and E. S. Yeung, *Chemical Communications*, 2011, 47, 11981-11983.
6. L. Shang, R. M. Dorlich, S. Brandholt, R. Schneider, V. Trouillet, M. Bruns, D. Gerthsen and G. U. Nienhaus, *Nanoscale*, 2011, 3, 2009-2014.

7. M. Yu, C. Zhou, J. Liu, J. D. Hankins and J. Zheng, *Journal of the American Chemical Society*, 2011, 133, 11014-11017.

8. C. Zhou, M. Long, Y. Qin, X. Sun and J. Zheng, *Angewandte Chemie - International Edition*, 2011, 50, 3168-3172.

9. J. Liu, M. Yu, C. Zhou, S. Yang, X. Ning and J. Zheng, *Journal of the American Chemical Society*, 2013, 135, 4978-4981.

10. J. P. Wilcoxon and B. L. Abrams, *Chemical Society Reviews*, 2006, 35, 1162-1194.

11. J. Zheng, P. R. Nicovich and R. M. Dickson, *Annual Review of Physical Chemistry*, 2007, 58, 409-431.

12. J. Zheng, C. Zhou, M. Yu and J. Liu, *Nanoscale*, 2012, 4, 4073-4083.

13. R. Jin, *Nanoscale*, 2010, 2, 343-362.

14. N. Cathcart and V. Kitaev, *Journal of Physical Chemistry C*, 2010, 114, 16010-16017.

15. T. Gregory Schaaff and R. L. Whetten, *Journal of Physical Chemistry B*, 2000, 104, 2630-2641.

16. L. A. Angel, L. T. Majors, A. C. Dharmaratne and A. Dass, *ACS Nano*, 2010, 4, 4691-4700.

17. S. H. Cha, J. U. Kim, K. H. Kim and J. C. Lee, *Chemistry of Materials*, 2007, 19, 6297-6303.

18. T. Ohta, M. Shibuta, H. Tsunoyama, Y. Negishi, T. Eguchi and A. Nakajima, *Journal of Physical Chemistry C*, 2013, 117, 3674-3679.

19. I. Díez, M. Pusa, S. Kulmala, H. Jiang, A. Walther, A. S. Goldmann, A. H. E. Müller, O. Ikkala and R. H. A. Ras, *Angewandte Chemie - International Edition*, 2009, 48, 2122-2125.

20. L. Shang and S. Dong, *Chemical Communications*, 2008, 1088-1090.

21. J. Zhang, S. Xu and E. Kumacheva, *Advanced Materials*, 2005, 17, 2336-2340.

22. J. Zheng, C. Zhang and R. M. Dickson, *Physical Review Letters*, 2004, 93, 077402-077401-077402-077404.

23. J. Sharma, H. C. Yeh, H. Yoo, J. H. Werner and J. S. Martinez, *Chemical Communications*, 2010, 46, 3280-3282.

24. E. G. Gwinn, P. O'Neill, A. J. Guerrero, D. Bouwmeester and D. K. Fygenson, *Advanced Materials*, 2008, 20, 279-283.

25. C. I. Richards, S. Choi, J. C. Hsiang, Y. Antoku, T. Vosch, A. Bongiorno, Y. L. Tzeng and R. M. Dickson, *Journal of the American Chemical Society*, 2008, 130, 5038-5039.

26. Y. Negishi, K. Nobusada and T. Tsukuda, *Journal of the American Chemical Society*, 2005, 127, 5261-5270.

27. X. Le Guevel, V. Trouillet, C. Spies, K. Li, T. Laaksonen, D. Auerbach, G. Jung and M. Schneider, *Nanoscale*, 2012, 4, 7624-7631.

28. C. L. Liu, H. T. Wu, Y. H. Hsiao, C. W. Lai, C. W. Shih, Y. K. Peng, K. C. Tang, H. W. Chang, Y. C. Chien, J. K. Hsiao, J. T. Cheng and P. T. Chou, *Angewandte Chemie - International Edition*, 2011, 50, 7056-7060.

29. A. Baksi, P. L. Xavier, K. Chaudhari, N. Goswami, S. K. Pal and T. Pradeep, *Nanoscale*, 2013, 5, 2009-2016.

30. K. Chaudhari, P. L. Xavier and T. Pradeep, *ACS Nano*, 2011, 5, 8816-8827.

31. X. Le Guevel, N. Daum and M. Schneider, *Nanotechnology*, 2011, 22.

32. S. M. Lystvet, S. Volden, G. Singh, M. Yasuda, O. Halskau and W. R. Glomm, *RSC Advances*, 2013, 3, 482-495.

33. J. Xie, Y. Zheng and J. Y. Ying, *Journal of the American Chemical Society*, 2009, 131, 888-889.

34. M. Zhu, C. M. Aikens, F. J. Hollander, G. C. Schatz and R. Jin, *Journal of the American Chemical Society*, 2008, 130, 5883-5885.

35. K. M. Harkness, D. E. Cliffel and J. A. McLean, *Analyst*, 2010, 135, 868-874.

36. K. M. Harkness, L. S. Fenn, D. E. Cliffel and J. A. McLean, *Analytical Chemistry*, 2010, 82, 3061-3066.

37. O. Varnavski, G. Ramakrishna, J. Kim, D. Lee and T. Goodson, *Journal of the American Chemical Society*, 2010, 132, 16-17.

38. H. C. Weissker and C. Mottet, *Physical Review B - Condensed Matter and Materials Physics*, 2011, 84.

39. B. Bellina, I. Compagnon, F. Bertorelle, M. Broyer, R. Antoine, P. Dugourd, L. Gell, A. Kulesza, R. Mitrić and V. Bonačić-Koutecký, *Journal of Physical Chemistry C*, 2011, 115, 24549-24554.

40. C. M. Aikens, *Journal of Physical Chemistry C*, 2008, 112, 19797-19800.

41. Z. Wu, J. Chen and R. Jin, *Advanced Functional Materials*, 2011, 21, 177-183.

42. O. Toikkanen, S. Carlsson, A. Dass, G. Rönnholm, N. Kalkkinen and B. M. Quinn, *Journal of Physical Chemistry Letters*, 2010, 1, 32-37.

43. O. Toikkanen, V. Ruiz, G. Rönnholm, N. Kalkkinen, P. Liljeroth and B. M. Quinn, *Journal of the American Chemical Society*, 2008, 130, 11049-11055.

44. J. T. V. Wijngaarden, O. Toikkanen, P. Liljeroth, B. M. Quinn and A. Meijerink, *Journal of Physical Chemistry C*, 2010, 114, 16025-16028.

45. R. L. Donkers, D. Lee and R. W. Murray, *Langmuir*, 2004, 20, 1945-1952.

46. P. R. Nimmala, B. Yoon, R. L. Whetten, U. Landman and A. Dass, *Journal of Physical Chemistry A*, 2013, 117, 504-517.

47. H. Qian, M. Zhu, Z. Wu and R. Jin, *Accounts of Chemical Research*, 2012, 45, 1470-1479.

48. G. Wang, R. Guo, G. Kalyuzhny, J. P. Choi and R. W. Murray, *Journal of Physical Chemistry B*, 2006, 110, 20282-20289.

49. Z. Wu and R. Jin, *Nano Letters*, 2010, 10, 2568-2573.

50. C. Zhou, C. Sun, M. Yu, Y. Qin, J. Wang, M. Kim and J. Zheng, *Journal of Physical Chemistry C*, 2010, 114, 7727-7732.

51. K. Susumu, H. T. Uyeda, I. L. Medintz, T. Pons, J. B. Delehanty and H. Mattoussi, *Journal of the American Chemical Society*, 2007, 129, 13987-13996.

52. B. C. Mei, K. Susumu, I. L. Medintz and H. Mattoussi, *Nature protocols*, 2009, 4, 412-423.

53. K. Susumu, B. C. Mei and H. Mattoussi, *Nature protocols*, 2009, 4, 424-436.

54. K. Susumu, E. Oh, J. B. Delehanty, J. B. Blanco-Canosa, B. J. Johnson, V. Jain, W. J. Hervey, W. R. Algar, K. Boeneman, P. E. Dawson and I. L. Medintz, *Journal of the American Chemical Society*, 2011, 133, 9480-9496.

55. C. A. J. Lin, T. Y. Yang, C. H. Lee, S. H. Huang, R. A. Sperling, M. Zanella, J. K. Li, J. L. Shen, H. H. Wang, H. I. Yeh, W. J. Parak and W. H. Chang, *ACS Nano*, 2009, 3, 395-401.

56. F. Aldeek, M. A. H. Muhammed, G. Palui, N. Zhan and H. Mattoussi, *ACS Nano*, 2013, 7, 2509-2521.

57. M. A. H. Muhammed, F. Aldeek, G. Palui, L. Trapiella-Alfonso and H. Mattoussi, *ACS Nano*, 2012, 6, 8950-8961.

58. E. Oh, F. K. Fatemi, M. Currie, J. B. Delehanty, T. Pons, A. Fragola, S. Lévêque-Fort, R. Goswami, K. Susumu, A. L. Huston and I. L. Medintz, *Particle and Particle Systems Characterization*, 2013, 30, 453-466.

59. G. Carotenuto and L. Nicolais, *Journal of Materials Chemistry*, 2003, 13, 1038-1041.

60. Y. Levi-Kalisman, P. D. Jadzinsky, N. Kalisman, H. Tsunoyama, T. Tsukuda, D. A. Bushnell and R. D. Kornberg, *Journal of the American Chemical Society*, 2011, 133, 2976-2982.

61. X. Dong, J. Cheng, J. Li and Y. Wang, *Analytical Chemistry*, 2010, 82, 6208-6214.

62. A. Dass, A. Stevenson, G. R. Dubay, J. B. Tracy and R. W. Murray, *Journal of the American Chemical Society*, 2008, 130, 5940-5946.

63. X. Lou, B. F. M. De Waal, J. L. J. Van Dongen, J. A. J. M. Vekemans and E. W. Meijer, *Journal of Mass Spectrometry*, 2010, 45, 1195-1202.

64. C. Vericat, G. A. Benitez, D. E. Grumelli, M. E. Vela and R. C. Salvarezza, *Journal of Physics Condensed Matter*, 2008, 20.

65. M. P. Casaletto, A. Longo, A. Martorana, A. Prestianni and A. M. Venezia, *Surface and Interface Analysis*, 2006, 38, 215-218.

66. M. Zhu, W. T. Eckenhoff, T. Pintauer and R. Jin, *Journal of Physical Chemistry C*, 2008, 112, 14221-14224.

67. S. Link, A. Beeby, S. FitzGerald, M. A. El-Sayed, T. G. Schaaff and R. L. Whetten, *Journal of Physical Chemistry B*, 2002, 106, 3410-3415.

68. M. A. H. Muhammed, S. Ramesh, S. S. Sinha, S. K. Pal and T. Pradeep, *Nanoresearch*, 2008, 1, 333-340.

69. R. Jin, H. Qian, Z. Wu, Y. Zhu, M. Zhu, A. Mohanty and N. Garg, *Journal of Physical Chemistry Letters*, 2010, 1, 2903-2910.

70. X. Tu, W. Chen and X. Guo, *Nanotechnology*, 2011, 22.

71. M. S. Devadas, V. D. Thanthirige, S. Bairu, E. Sinn and G. Ramakrishna, *Journal of Physical Chemistry C*, 2013, 117, 23155-23161.

72. X. Wen, P. Yu, Y. R. Toh and J. Tang, *Journal of Physical Chemistry C*, 2012, 116, 11830-11836.

73. X. Wen, P. Yu, Y. R. Toh and J. Tang, *Journal of Physical Chemistry C*, 2013, 117, 3621-3626.

74. A. M. Jackson, J. W. Myerson and F. Stellacci, *Nature Materials*, 2004, 3, 330-336.

75. M. C. Daniel and D. Astruc, *Chemical Reviews*, 2004, 104, 293-346.

76. C. Bullen and P. Mulvaney, *Langmuir*, 2006, 22, 3007-3013.

77. P. T. K. Chin, M. Van Der Linden, E. J. Van Harten, A. Barendregt, M. T. M. Rood, A. J. Koster, F. W. B. Van Leeuwen, C. De Mello Donega, A. J. R. Heck and A. Meijerink, *Nanotechnology*, 2013, 24.

78. L. Shang, S. Dong and G. U. Nienhaus, *Nano Today*, 2011, 6, 401-418.

79. G. A. Simms, J. D. Padmos and P. Zhang, *Journal of Chemical Physics*, 2009, 131.

80. G. W. Shu, C. C. Lin, H. P. Chung, J. L. Shen, C. A. J. Lin, C. H. Lee, W. H. Chang, W. H. Chan, H. H. Wang, H. I. Yeh, C. T. Yuan and J. Tang, *Applied Physics Letters*, 2009, 95, 261911-261911-261914.

81. J. Park, J. Nam, N. Won, H. Jin, S. Jung, S. Jung, S. H. Cho and S. Kim, *Advanced Functional Materials*, 2011, 21, 1558-1566.

82. J. H. Scofield, *Journal of Electron Spectroscopy and Related Phenomena*, 1976, 8, 129-137.

Nanoscale Accepted Manuscript